Final Report • 26 September 2012

Spin-Precession Organic Magnetic Sensor

SRI Project P19028

ONR Contract N00014-09-C-0292

Prepared by:

Srini Krishnamurthy, Senior Principal Scientist
Applied Physical Sciences Laboratory

Prepared for:

Office of Naval Research
Code 321MS
875 N. Randolph Street
Arlington VA 22203-1995

Attention: Stephen Potashnik

Report Documentation Page

Form Approved
OMB No. 0704-0188

1. REPORT DATE	2. REPORT TYPE	3. DATES COVERED
26 SEP 2012		**00-00-2012 to 00-00-2012**

4. TITLE AND SUBTITLE	5a. CONTRACT NUMBER
Spin-Precession Organic Magnetic Sensor	5b. GRANT NUMBER
	5c. PROGRAM ELEMENT NUMBER
6. AUTHOR(S)	5d. PROJECT NUMBER
	5e. TASK NUMBER
	5f. WORK UNIT NUMBER
7. PERFORMING ORGANIZATION NAME(S) AND ADDRESS(ES) **SRI International,333 Ravenswood Avenue,Menlo Park,CA, 94025**	8. PERFORMING ORGANIZATION REPORT NUMBER
9. SPONSORING/MONITORING AGENCY NAME(S) AND ADDRESS(ES)	10. SPONSOR/MONITOR'S ACRONYM(S)
	11. SPONSOR/MONITOR'S REPORT NUMBER(S)

12. DISTRIBUTION/AVAILABILITY STATEMENT
Approved for public release; distribution unlimited

13. SUPPLEMENTARY NOTES

14. ABSTRACT

15. SUBJECT TERMS

16. SECURITY CLASSIFICATION OF:			17. LIMITATION OF ABSTRACT	18. NUMBER OF PAGES	19a. NAME OF RESPONSIBLE PERSON
a. REPORT	b. ABSTRACT	c. THIS PAGE			
unclassified	**unclassified**	**unclassified**	**Same as Report (SAR)**	**25**	

CONTENTS

EXECUTIVE SUMMARY

SRI International, in collaboration with Professor Jing Shih of the University of California-Riverside (UCR), Professor Nathan Newman of Arizona State University (ASU), and Professor Edmond Nowak of the University of Delaware (UD), has been funded (from June 2009 through September 2012) through ONR Contract (N00014-09-C-0292) to fabricate a magnetic sensor with a half-metallic ferromagnet (FM) contact and polymers and demonstrate its sensing capability. In this study we considered $La_{0.7}Sr_{0..3}MnO_3$ (LSMO) and $CoFe_{50}Al_{25}Si_{25}$ (CFAS) alloys for half-metallic FM contacts and poly(3,4-ethylenedioxythiophene) (PEDOT) and poly-3(hexylthiophene) (P3HT) for polymers. Room temperature operation of this ultrasensitive device requires half-metallic ferromagnetic contacts with high Curie temperature (T_c), ultra-low-mobility polymer with very high doping density, nano-scale trenches, successful charge and spin injection into polymers from FM half-metal contacts, and spin precession in polymers. The FM films for vertical and lateral devices were grown at UCR and ASU, respectively. Most device fabrication was carried out at SRI, while magnetic and noise measurements were performed at ASU and UD.

In a previous ONR-funded program (N00014-07-C-0393), ASU had used pulsed laser deposition (PLD) and demonstrated (a) growth of high-quality LSMO with critical temperature T_c >360 K and metal-semiconductor transition temperature, T_{MS} > 400 K; (b) charge and spin injection from LSMO into low-mobility polymers; and (c) high magnetoresistance (MR) in micron-thick polymer devices. The results were published in the literature.[1].

In the current program, UCR used a DC magnetron sputtering growth method to improve the surface quality of the LSMO films while maintaining high-quality electrical and magnetic properties. We modified our device design from a lateral to a vertical structure to increase the device area and improve the LSMO/polymer interface quality for charge injection. We further carried out a systematic study to understand polymer deposition and processing. We modified the fabrication procedure to address the issues related to device stability and charge injection and applied the fabrication sequence to Co/polymer/Co for validation. First, we fabricated several devices with LSMO and polymer (P3HT) and evaluated the magnetic sensor operation. Although spin precession, a requirement for ultra-high sensitivity, could be observed at low temperature, the device performance at room temperature was still dominated by noise. The cause of increased noise is the associated decrease in contract magnetization. Since LSMO has a T_c that is only slightly higher than room temperature (RT), the magnetization at RT is very small, thus reducing the signal. In our local device, where both current and voltage are measured between the same two terminals, the resistance changed with time, resulting in increased noise. Consequently, the signal-to-noise ratio (SNR) is too small for acceptable sensor performance.

[1] Tezuka et al., *Appl. Phys. Lett.* **95**, 232507, 2009.

Based on the knowledge acquired in our studies, we identified the CFAS as the half-metallic FM with very high RT magnetization for improved signal, and a nonlocal device design for reduced noise. We (a) grew CFAS layers by both PLD and magnetron sputtering; (b) measured magnetic properties of CFAS layers; (c) measured surface polarization by Andreev reflections; (d) fabricated local and non-local devices; and (e) deposited both P3HT and PEDOT polymers with and without a tunnel barrier. The layers grown at ASU were demonstrated to have far superior magnetic properties: high coercive field (~ 450 Oe), large magnetization (~ 2000 emu/cc), low electrical and magneto resistance (~50 μΩ-cm), large spin polarization (p ~ 0.73), high critical temperature (~1000 K), and insignificant temperature dependence of the magnetization. Both PLD-grown and sputtered samples were found to have magnetic properties superior to the published values. The sputtered samples have larger bulk magnetization than PLD-grown samples but have similar coercive fields. The Andreev reflection measurements clearly show that the surface polarization in PLD-grown CFAS is ~ 60%, and in sputtered CFAS it is ~ 73% at RT. These values are the highest ever reported in *any* magnetic material. We used focused ion beam lithography to fabricate both local and nonlocal CFAS devices and deposited a highly conductive polymer PEDOT or semiconducting P3HT on our device. We developed an AC lock-in measurement technique to improve SNR. None of the devices have showed any reliable magnetic response at RT.

Our analysis indicates that (a) resistance mismatch between the contact and the polymer is possibly too large to allow spin injection and (b) the natural oxide in the tunnel junction, grown to alleviate the resistance mismatch issue, is interacting with the tunneling electrons, possibly destroying spin polarization. Further studies for demonstration of enhanced magnetic response should use sputtered CFAS samples with controlled and noninteracting oxide thickness.

TECHNICAL DISCUSSION

1. Objectives

Our long-term goal is to develop an ultrasensitive, room temperature, compact magnetic sensor based on spin precession. The specific aim of this study was to fabricate a magnetic sensor device using a half-metal—$La_{0.7}Sr_{0.3}MnO_3$ (LSMO) or $CoFe_{50}Al_{25}Si_{25}$ (CFAS)— as ferromagnetic (FM) contacts and a polymer—poly(3,4-ethylenedioxythiophene) (PEDOT) or poly-3(hexylthiophene) (P3HT)—as transport medium to demonstrate and optimize the sensing capability of the device. The sensitivity depends crucially on spin injection efficiency and duration of spin relaxation time. The half-metallicity ensures high spin injection, and the small spin-orbit interaction in polymers ensures long spin lifetimes.

The immediate objectives of this effort are to (a) improve the magnetic sensor device design based on the results obtained under a previous ONR-funded effort; (b) fabricate both local and nonlocal LSMO and CFAS-based nanostructures for testing and characterization; (c) use previously developed polymers that meet the mobility and carrier density requirements and deposit them into devices; (d) measure electrical and magneto resistance; and (e) measure magnetic sensing performance for operation at RT.

2. Device Fundamentals

2.1 Concept

The device we considered contains half-metal magnetic contacts and polymer as the charge transport medium. The contacts are magnetically poled to achieve parallel magnetization. The half-metal nature of the contact allows injection of only one kind of spin (parallel to the magnetization) into the organic material. The constituents of the organics are usually atoms with small atomic numbers (such as H, C, N, O, and S), and the spin-orbit coupling is extremely small, which allows the injected spins to stay coherent for long times. In the absence of any magnetic field, the injected electrons will retain the spin and can find a state in the other contact, resulting in sizable current. However, when a magnetic field is applied, the electron spin will precess, and its spin orientation will change with reference to the contact magnetization, resulting in an increased resistance (and reduced current). Since a very small magnetic field is required to alter the electron spin orientation, the device is predicted to have very high sensitivity—a few $fT/Hz^{1/2}$— even in RT operation.

2.2 Requirements

The magnetic field sensitivity of the device depends on our ability to (a) inject only one kind of spin, known as spin injection efficiency, (b) maintain the spin coherence over the device length,

and (c) choose a transport medium for a longer device. The spin injection efficiency, η, has been predicted[2] to be dependent on injector resistance (R_L) and transport medium resistance (R_P) by

$$\eta = \frac{8p}{8 + 4\frac{R_P}{R_L}\left(1 - p^2\right)}$$

Note that when the polarization *p* is 1, then η is also 1, irrespective of the resistance mismatch across the interface. However, when *p* is not exactly 1, η depends sensitively on the ratio of the resistances R_p/R_L as shown in Figure 1.

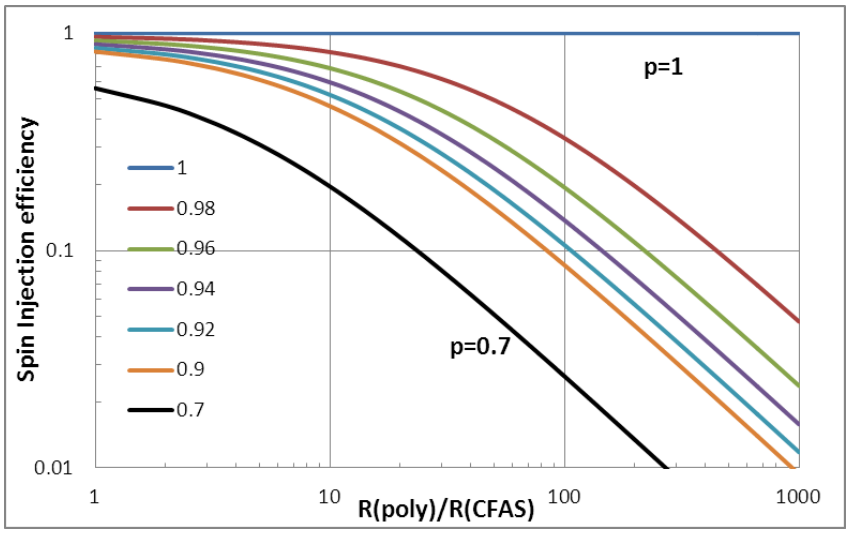

Figure 1: Predicted spin-injection efficiency.

It is clear that high injection can be obtained when the FM contacts are half-metals (*p*=1). Hence we consider LSMO and CFAS, which are predicted to be good half-metals (i.e., *p* large but not equal to 1) through surface emission or magnetic tunnel junction studies. The spin polarization, particularly of the electrons from the surface that are injected into the device, can be directly determined by Andreev's reflection measurements. The transport medium is chosen to be polymers, because they have light atoms with little or no spin-orbit interaction and hence electron spin coherence can be maintained over longer distance (~ a few μm). In particular, the ultra-low mobility of charge carrier in the polymers will lead to long transit times. Hence a small applied magnetic field will result in a large change in electron spin orientation, which results in larger resistance change and enhanced sensitivity. However, as seen from Figure 1, polymer resistance will need to be matched to the contact resistance. Noting that the ratio of spin diffusion length in polymer to that in the FM contact can be ~10^3, their resistivity ratio needs to be ~10^{-3}. Since the resistivity of FM metals are ~10^{-5} Ω-cm, polymer resistivity is required to be 10^{-2} Ω-cm. Even with 10^{19} cm^{-3} doping, the polymer resistivity will be 10^4 Ω-cm (because of low

[2] Schmidt, *Phys. Rev.* B**62,** 4790, 2000.

mobility ~10^{-4} cm^2/Vs). Hence, it is clear that the resistance match can be obtained only when the contact resistance is increased—possibly with a tunnel barrier between the FM metal and the polymer. However, this barrier thickness must be carefully chosen as a tradeoff between increased spin injection efficiency and decreased charge injection efficiency.

3. Device Configurations

We considered both vertical and lateral device architectures, as each offered distinct advantages. Owing to their larger area, the vertical devices are expected to have higher sensitivity but require high-temperature deposition of FM metal on polymers. The lateral devices are easier to fabricate but have limited sensitivity.

3.1 Vertical Devices

A schematic of the vertical device is shown in Figure 2 (left). The bottom substrate has an LSMO (blue) layer, gold contact (red), and a 1-µm-tall SiO_2 well (green) that will be top-filled with polymer (yellow). Another Strontium Tin Oxide substrate with Au will be placed on top and sealed to form a vertical device. The polymer-well area is the device area. This design has several advantages: (1) the LSMO surfaces are never subjected to any structural damage, and so spin injection at RT should reach its maximum; (2) the device area increases (from 200 μm^2 currently to 1 mm^2), and so the signal should also increase linearly; (3) the area increase will also decrease noise (as a square root of area), and hence the sensitivity should increase by several orders of magnitude; and (4) it enables us to develop a sensor array for further improvement in signal and sensitivity at lower frequencies. A preliminary version of the device fabricated for a proof-of-concept demonstration is shown in Figure 2 (right). The screws were used to keep the top LSMO in good contact with the polymer.

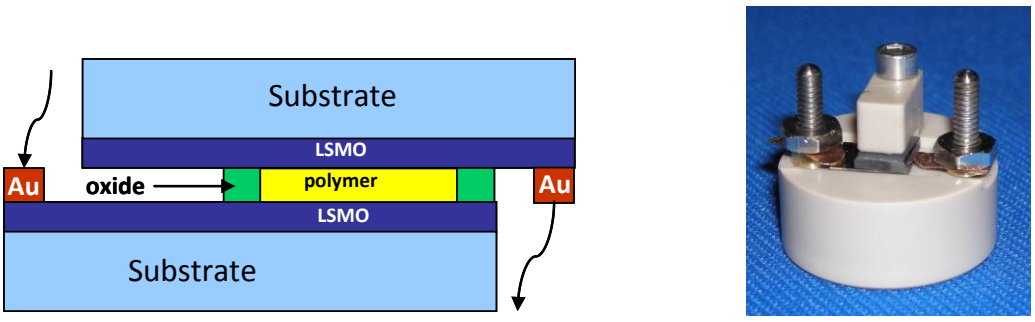

Figure 2: Schematic diagram of the vertical device (left) and a fabricated device (right).

3.2 Lateral Devices

Lateral devices are easier to fabricate because they require high-quality deposition of the FM layer and focused ion beam lithography to etch the trench for polymer deposition. If the aspect ratio of the trench is large, the uniform filling by polymer will be hard to achieve. A careful

design is required to enable polymer filling while staying within the spin coherence length in polymer. We chose a design, as shown schematically in Figure 3, that enables both local and nonlocal measurements. We expected considerable noise reduction from the nonlocal configuration. The terminals 1 (T1) through 4 (T4) are FM strips (in the z direction) on a substrate with carefully chosen widths (W_i) and separated by selected distances (d_{ij}). The polymer is drop-cast on FM lines. The FM contacts are magnetized. A constant current is supplied between T1 and T2. For local measurements, the change in voltage with magnetic (H) field is also measured between terminals T1 and T2. In nonlocal configuration, the voltage is measured between terminals T3 and T4 as shown. Depending on the magnetization of T2, charge carrier spins (parallel to the magnetization) accumulate under T2 and diffuse toward T3 and T4. In a steady-state distribution of spins, the potential measured between T3 and T4 depends on the density of carriers with spins parallel to their respective contact magnetization at T3 and T4. Since this is an open circuit voltage, no charge transport between T3 and T4 takes place. Consequently, the interface issues no longer contribute to noise. This material and design thus potentially increase the signal and decrease noise, thus likely enabling high-sensitivity operation at RT.

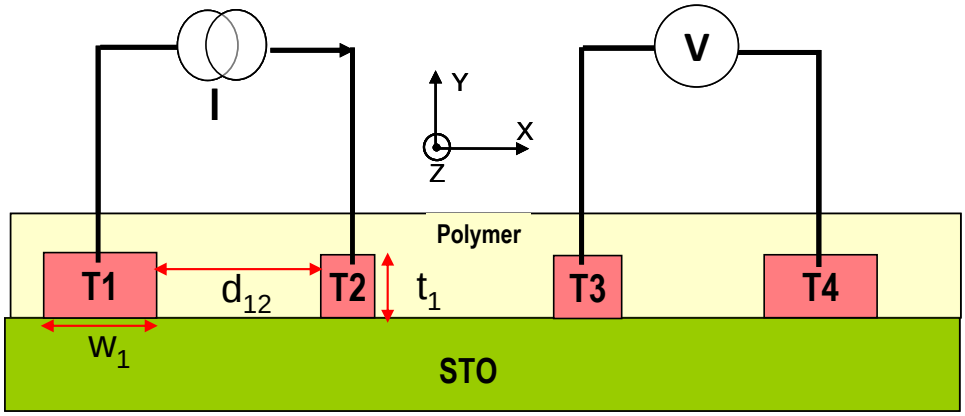

Figure 3: Schematic nonlocal CFAS device.

Figure 4 shows the fabricated device with CFAS strips and polymer. The values of W_i are 20 μm, 1.0 μm, 0.5 μm, and 20 μm, respectively, for i=1, 2, 3, 4. The strips are 1 μm apart. In local device configuration the voltage is measured between terminals 1 and 2, and in nonlocal device configuration between terminals 3 and 4. To ensure that current flows only between the CFAS and polymer, the size of the polymer dot should be small enough not to touch the numbered Au pads. A scanning electron microscope (SEM) picture of a fabricated device with micron-sized polymer dot—PEDOT—deposited by Rainmaker is shown at left in Figure 4. We have fabricated several devices with different (a) growth methods, (b) substrates, (c) growth/ anneal temperatures, and (d) tunnel-oxide layer thicknesses.

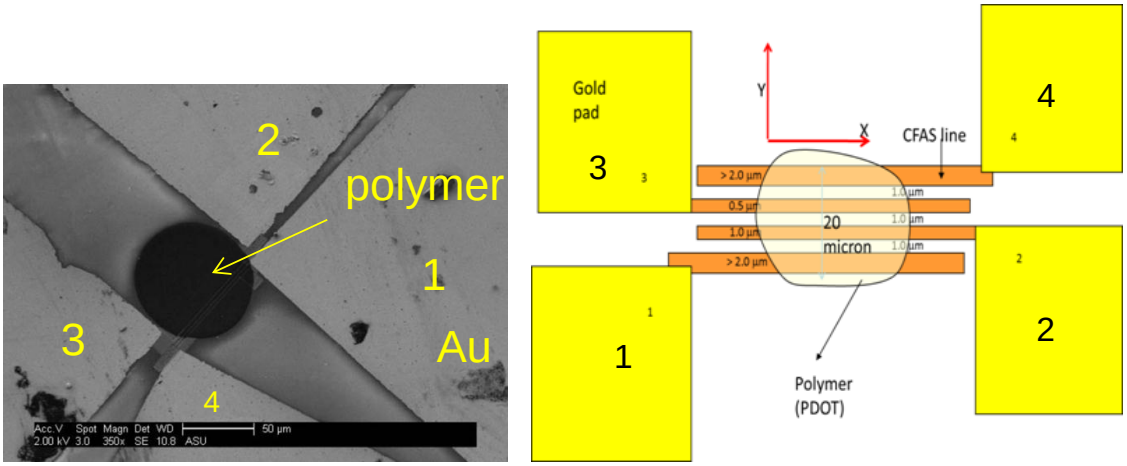

Figure 4: Fabricated CFAS structure with polymer (left) and corresponding schematic diagram (right).

4. Growth and Characterization

4.1 LSMO

Although the PLD method used in the previously funded ONR program yielded LSMO films with high-quality electrical and magnetic properties, the surface was rough and the interface between LSMO and polymer was not uniform. The associated change in lattice structure on the surface is known to have a negative effect on surface spin polarization and injection. To obtain smooth films, and hence enhance spin injection, we chose the DC magnetron sputtering method to grow LSMO at UCR. These films have demonstrated an ultra-smooth surface, in addition to previously demonstrated high-quality electrical and magnetic properties.

4.2 CFAS

Both LSMO and CFAS are characterized for magnetic properties such as Curie temperature, coercive field, and magnetization. When a ferromagnetic film is placed in the H field, it is magnetized. The change of magnetic moment (M) with H displays a hysteresis curve as shown in Figure 5. The field where M shows a steep increase is denoted as coercive field H_c, and the value of M at zero H field is denoted as magnetization M_s. In the literature,[1] the alloy $Co_2FeAl_{0.5}Si_{0.5}$ (CFAS) has been demonstrated to have M_s of ~1100 emu/cc and H_c of ~ 40 Oe at RT. More important,

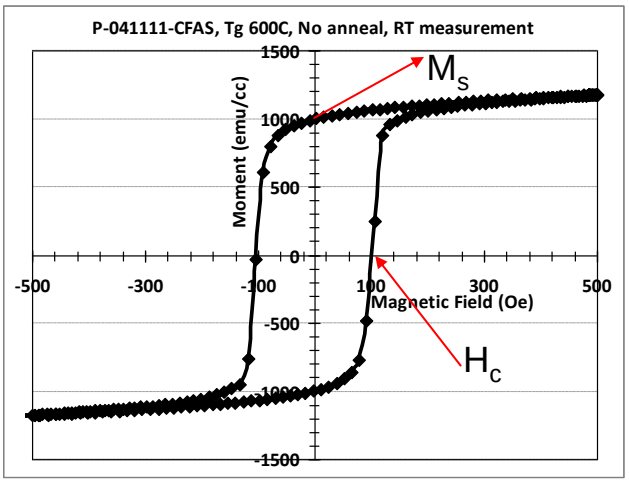

Figure 5: Measured hysteresis curve of CFAS grown by PLD at 600 °C.

both M_s and H_c are found to be temperature independent, suggesting the possibility of using CFAS for RT magnetic sensor operation. We grew CFAS samples by two growth methods—PLD and sputtering— and evaluated the magnetic properties of the films against state-of-the-art values.

4.2.1 Pulsed Laser Deposition

First we chose the PLD method to grow CFAS in two ways: a one-step process in which the growth temperature, T_g, is varied for optimum growth, and a two-step process in which a CFAS layer is deposited at RT but annealed at various temperatures, T_a, for optimum quality. We then evaluated the magnetic properties of the materials. The measured H_c and M_s are shown in Figure 6 and

Figure 7, respectively. The values obtained by the one-step (blue) and two-step (red) processes are compared with the best literature values.[1] We see that the coercive field (Figure 6) increases with temperature in both methods and that our values are always higher than the literature values. The larger coercive field is useful for magnetic sensor application by reducing the noise arising from H field fluctuations. Our measured value of M_s (Figure 7) increases with T_g non-monotonically (one-step process) and is nearly flat with T_a in the two-step process.

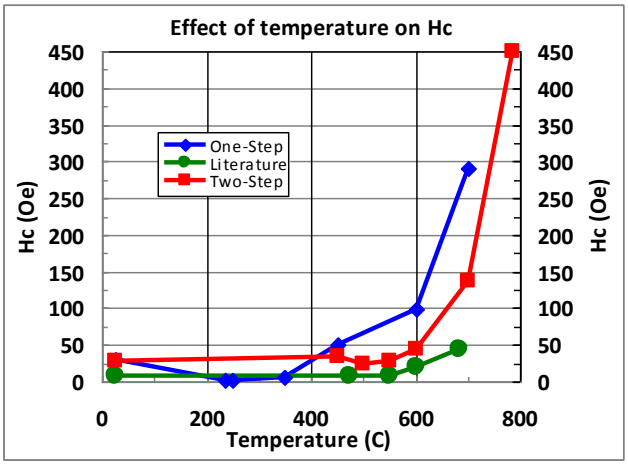

Figure 6: Measured coercive field of CFAS grown by PLD with one-step (blue) and two-step (red) process. Best literature [1] values are also shown (green).

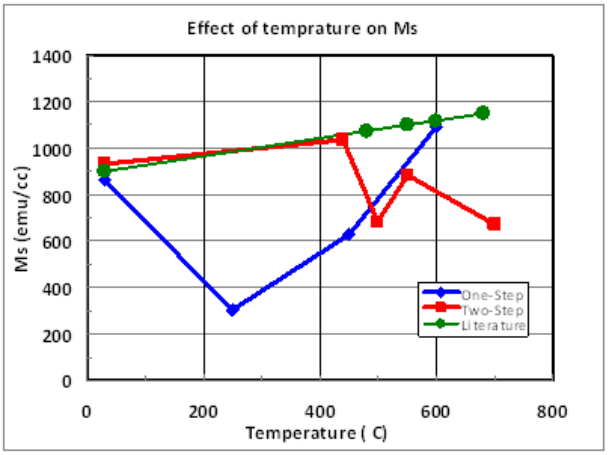

Figure 7: Measured magnetization of CFAS grown by PLD with one-step (blue) and two-step (red) process. Best literature [1] values are also shown (green).

Our estimated value of M_s is comparable to literature values at low T_a (or T_g). Our values using the one-step approach are lower initially, but reach the literature values at high T_g. The values obtained by our two-step process are comparable at low T_a, but show fluctuations at high T_a. The apparent fluctuation is caused by the error in estimating the thickness of the nonuniform layer grown by PLD. The literature values are obtained for smooth and flat CFAS layers grown by DC magnetron. For RT operation, the M_s and H_c should be large and should not change substantially

with temperature. To evaluate CFAS for sensor application, we measured magnetic moment as a function of magnetic field and temperature; the results are shown in Figure 8. We see that the coercive field and the magnetization change very little with T. Similar behavior was observed for all our samples.

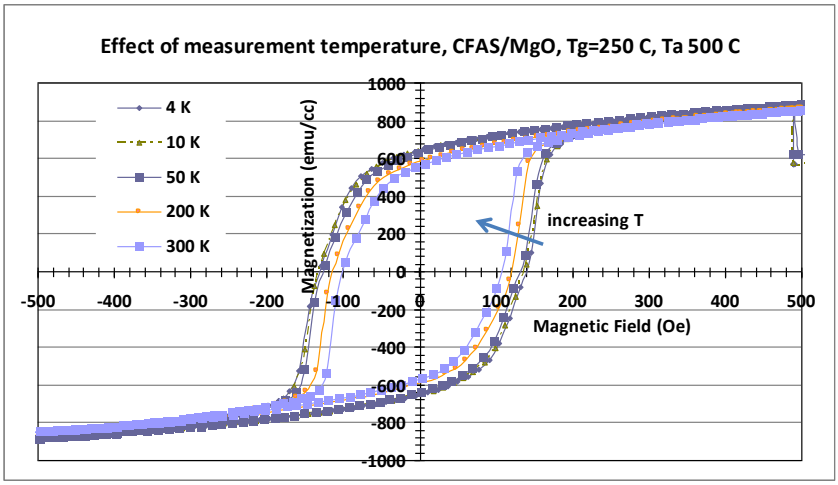

Figure 8: Measured hysteresis curves for various temperatures.

For CFAS to be used as contacts to inject and detect spins, it must have low electrical resistance (so that the resistance of the device is dominated by the polymer) and negligible magnetoresistance (MR) (so that the MR measured in the sensor arises mostly from the spin transport). We measured electrical resistance and MR of our CFAS thin films. As seen from Figure 9 and Figure 10, both resistances are very small and the changes with T or H are negligible, boding well for the use of CFAS as a ferromagnetic metal contact for our spin devices.

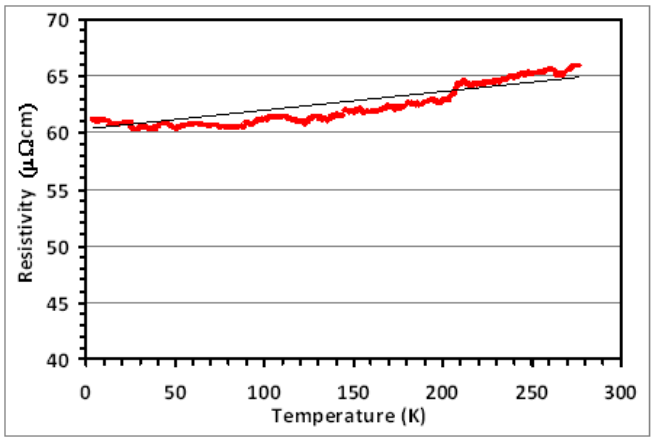

Figure 9: Measured electrical resistance of PLD-grown CFAS thin film.

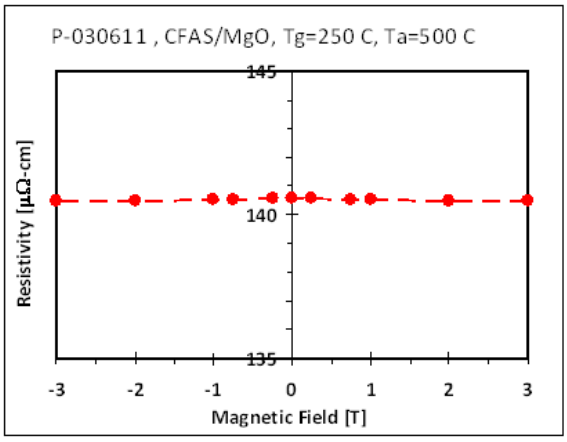

Figure 10: Measured magnetoresistance of PLD-grown CFAS thin film.

4.2.2 Sputtering

First, we chose the PLD method to grow CFAS and demonstrated a value of 100 Oe for H_c and 1100 emu/cc for M_s for a growth temperature of 600 ^oC. Then, we grew the samples with a sputtering process on two different substrates—MgO and Silicon thermal oxide (STO). As shown in Figure 11, the magnetic properties of the layers grown on STO are far superior to the values reported in the literature.[1] We obtained a value of 450 Oe for H_c and 2,000 emu/cc for M_s. Figure 12 and Figure 13 display the measured values of Hc and Ms on various samples. Sputtered samples on MgO (blue) are consistently better than PLD samples on MgO (green). In addition, the sputtered sample on STO (red) has much higher H_c and M_s than that grown on MgO (blue), and the optimum growth temperature is near 600 ^oC. We also grew samples at RT and annealed at high temperatures. The magnetic properties (not shown here) were consistently poorer than those grown at high temperature.

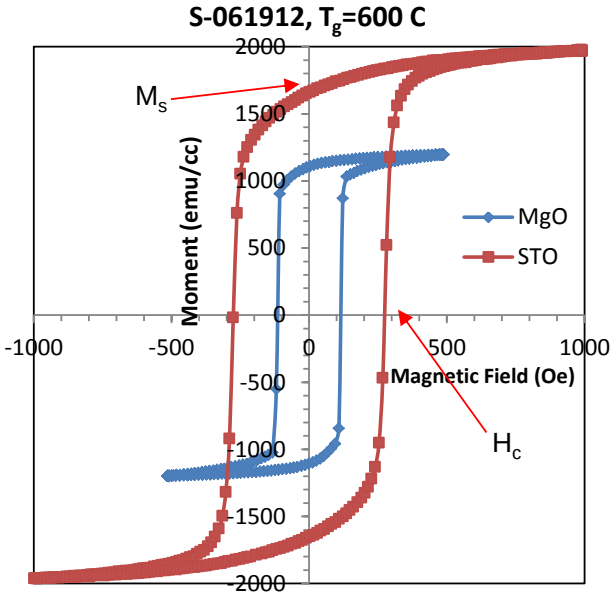

Figure 11: Measured hysteresis curve of 600 ^oC sputtered CFAS.

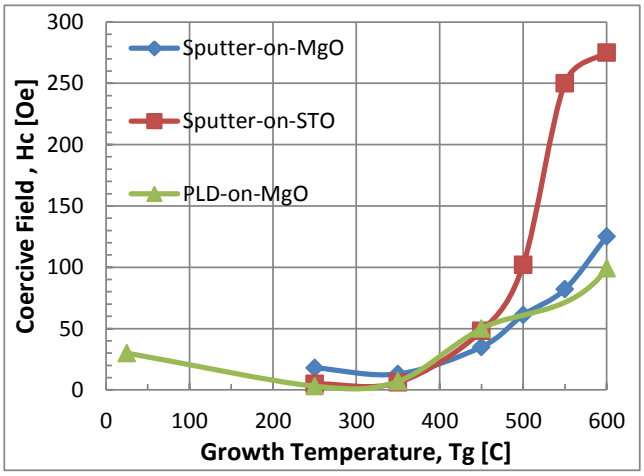

Figure 12: Measured coercive field of CFAS grown by PLD on MgO (green), sputtering on STO (blue), and sputtering on MgO.

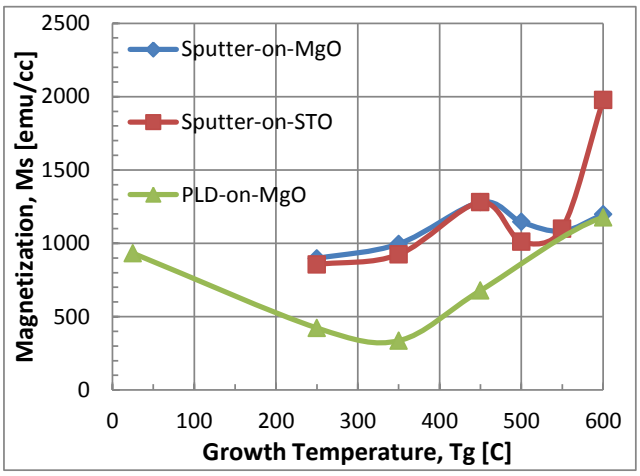

Figure 13: Measured magnetization of CFAS grown by PLD on MgO (green), sputtering on STO (blue), and sputtering on MgO.

Surface Polarization: The spin-injection efficiency is determined by the spin polarization at the surface/interface. For half-metals with defect-free surfaces, electrons with only one kind of spin are available for injection and the polarization factor, *p*, equals 1. In reality, ambient temperature

in relation to Curie temperature, surface oxidation, and lattice deformation can cause spin polarization at the surface to be lower, leading to a smaller value for *p*. The spin polarization factor, *p*, is the ratio of difference in up- and down-spin density to the total electron density. For example, Fe has 7 spin "up" electrons for every 3 spin "down" electrons and, equivalently, has a *p* value of 0.4. In the literature,[1] the CFAS has been interpreted to have a *p*=0.9 (or 90%). Although approximate values of *p* can be inferred from magnetic tunneling current measurements, a direct and accurate measurement can be obtained only from Andreev reflection (AR) studies. When an electron with energy less than the superconducting gap is injected from normal (N) metal into a superconductor (S), the hole of opposite spin will be reflected since S can accept only Cooper pairs. If N is pure half-metal, it does not have a hole of opposite spin, and the injection will not take place. By measuring the current as a function of applied bias, the surface spin polarization in N can be determined. The measured tunnel current as a function of applied bias is shown in Figure 14 for two samples with highest *p* value— PLD sample grown at 600 ºC (left) and sputtered CFAS (right). These samples are measured to have a *p* value of 0.6 (PLD) and 0.73 (sputtered).

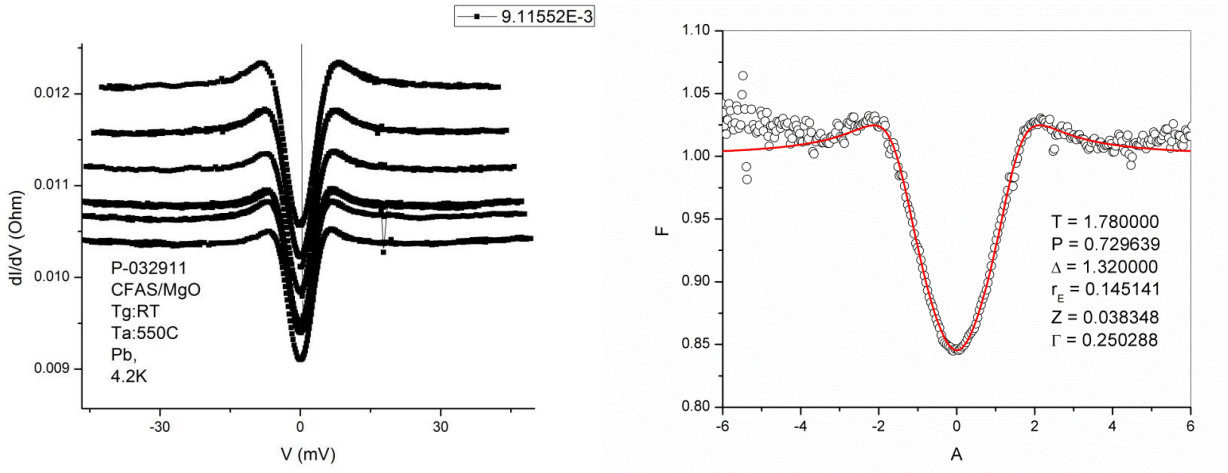

Figure 14: Measured Andreev reflection at 300 K from PLD-grown (left) and sputtered (right) CFAS.

We have systematically measured and listed the value of *p* by varying growth method, growth temperature, and substrates in Table 1. We see that polarization is high for higher anneal temperatures, and the highest value of *p* = 0.73 is obtained for CFAS sputtered on MgO at RT and annealed at 600 ^{o}C. This sample has large M_s and moderate H_c (also shown in Table 1). It is interesting to note that the highest bulk magnetic properties (H_c and M_s) are obtained when sputtered on STO at 600 ^{o}C. However, that sample showed the smallest *p* value of 0.35. The samples with best bulk magnetic properties are expected to have the highest spin polarization at the surface. The apparent discrepancy could be from the difference in surface preparation of the samples for Andreev reflection measurements.

Table 1: Surface spin polarization measured by Andreev reflection.

Sample #	substrate	Growth Method	Growth T (°C)	Annealing T (°C)	Thickness (°A)	Hc (Oe)	MS (emu/cc)	Polarization (AR results)
S-053012	MgO	sputtering	RT	No	493	30	689	45 %
S-053112	MgO	sputtering	RT	350	415	29	1434	40 %
S-060612	MgO	sputtering	RT	550	392	49	1172	60 %
S-060812	MgO	sputtering	RT	600	336	48	1230	**73 %**
S-061912	MgO	sputtering	600	No	303	125	1197	50 %
S-061912	SiO/Si	sputtering	600	No	303	275	1976	35 %
P-032911	MgO	PLD	RT	550	325	29	890	**60 %**
P-042511	MgO	PLD	RT	785	1008	450	762	50 %
Literature	Cr buffered MgO	MBE	200	400	50	-	-	**90% (inferred from TMR)**

Tunneling Barrier: With the value of p = 0.73 as shown above, we see from Figure 1 that a maximum spin efficiency of 60% is possible only if the resistances of the CFAS contact and the polymer are equal. With the CFAS resistivity of 100 μΩ-cm, the resistance match is possible only when the electrons are injected from CFAS through an oxide tunnel barrier. The tunneling process adds an effective resistance to the contact resistance. However, if the barrier thickness is too large, the injected current density will be too small for sensing measurements. Hence, a systematic tradeoff study is carried out.

Tunneling efficiency through the barrier is measured with a Pb probe at 4.2 K by applying a bias between the metal and the probe. Since Pb has a superconducting gap, the tunneling current is (ideally) zero until the bias aligns either the upper or the lower superconducting state with the metal Fermi level, and then current will increase linearly with bias. Accordingly, the conductance (dI/dV) will have a minimum at zero bias and maxima at bias corresponding to superconducting state energies. Classic I-V (red) and conductance (blue) curves are shown in Figure 15 (right). We have grown several CFAS samples with varying Al_2O_3 layer thickness d and measured I-V and conductance. The tunneling efficiency increased from 20% (at d = 5 nm) to 50% (at d = 2 nm). The highest tunneling efficiency of 80%, as shown in Figure 15 (left), is obtained when the barrier is a native oxide 2-nm thick. However, the measured conductance from this sample (blue) did not show peaks at conductance at superconducting state energies (as in the case of AR measurements shown in Figure 14), indicating that electrons interact with barrier (or surface states) on this sample while tunneling. For efficient spin injection, the oxide

layer on CFAS should be noninteracting, and hence studies of controlled Al_2O_3 layer thickness of 2 nm are required.

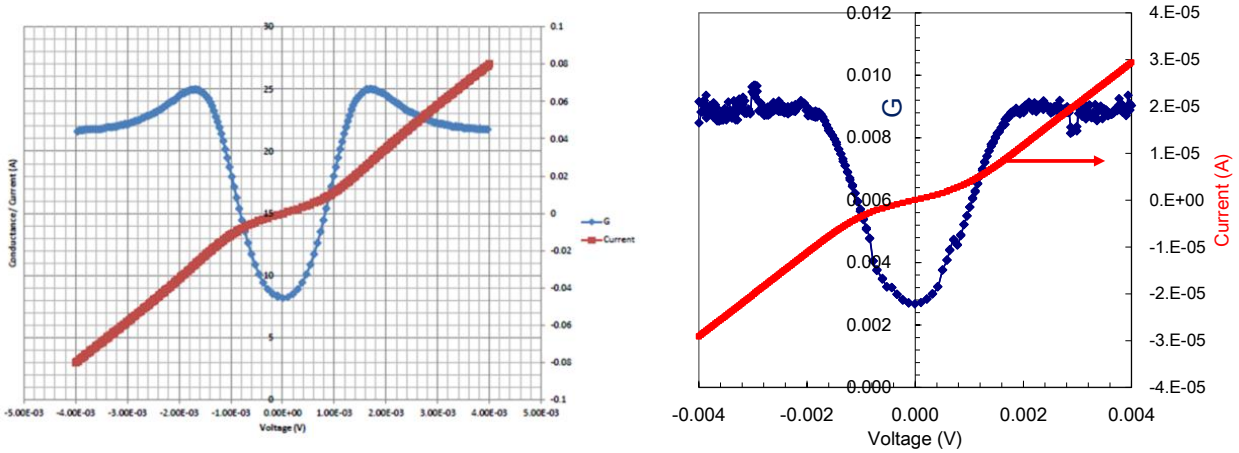

Figure 15: Measured tunneling current (red) and conductance (blue) of metal/oxide/Pb junction (left) and CFAS/oxide/Pb junction (right).

5. LSMO Device Results

5.1 Lateral Device

We have obtained a 300-nm-thick layer of LSMO using the PLD technique on lattice-matched $SrTiO_3$ substrates. The Curie temperature and metal-insulator temperature were measured and found to be ~350 K and ~380 K, respectively. In our approach, thin layers of Al_2O_3 and SiO_2 are deposited on LSMO, and reactive ion etching (RIE) is used to make a ~1-μm-wide trench in LSMO. Then, regioregular polythiophene (P3HT) polymer is deposited into the trench and Au contacts are made to the LSMO. The measured I-V curves indicated very good charge injection from LSMO into polymer, and the resistance varied substantially when the contact magnetization was increased with the application of a large magnetic field. We then placed the device in a 4-layer mu-metal shield and measured the resistance as a function of the small magnetic field applied perpendicular to the contact magnetization direction at 25 K. The measured resistances at fixed bias values of 1 V and 2 V are shown by data points in Figures 16 and 17, respectively. Solid lines show the resistance values calculated with known values of transport distance, conductivity, hole mobility in the polymer, and residual earth magnetic field within the 4-layer can. In the case of spin precession, the resistance will be an oscillatory function as seen in Figure 16 and Figure 17. Note that agreement is better at higher bias as signal increases with the voltage and we get a value of ~200 per tesla for the quantity $[V^{-1}(dV/dB)]$, which roughly translates into a sensitivity of 14 $nT/Hz^{1/2}$. However, we did not observe any oscillation at RT, and we see that the data is quite noisy even at low temperature.

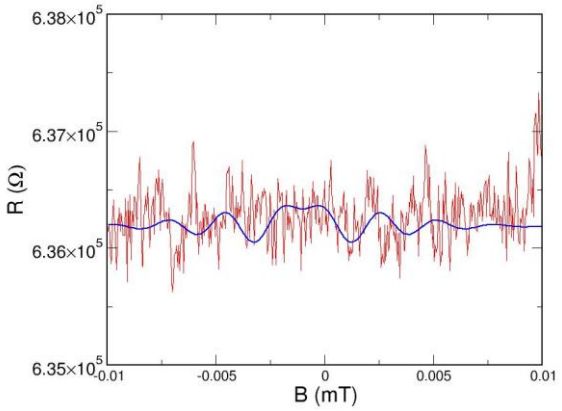

Figure 16: Measured resistance as a function of applied magnetic field and 1 V bias.

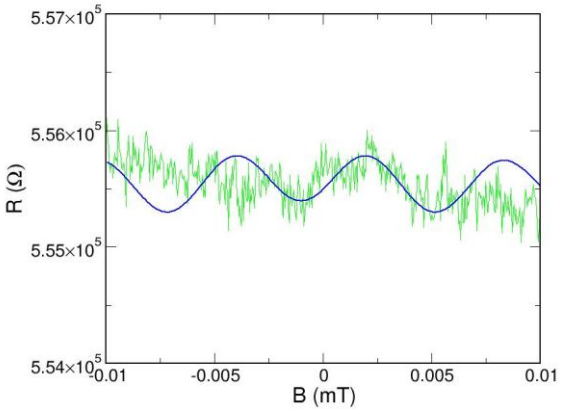

Figure 17: Measured resistance as a function of applied magnetic field and 2 V bias.

5.2 Vertical Device

For this study, Prof. Jing Shi at UCR grew high-quality LSMO layers. To identify the issues related to the fabrication of the vertical devices, we fabricated a preliminary device without any optimization control as follows.

1. Grow high-quality layers of LSMO by MBE on two $SrTiO_3$ substrates.
2. On one of the LSMO substrate, deposit 1-μm-thick SiO_2 with hard mask to cover the mm^2 of device area and metallization region.
3. Metallize both LSMO layers for ohmic contact.
4. Deposit P3HT and overfill the mm^2 of device area.
5. Flip the other LSMO piece over and make a sandwich structure (Figure 2, left).
6. Gently clamp both pieces together to ensure electrical contact by measuring I-V characteristics (Figure 2, right).

The presence of SiO_2 outside the device area restricted the current flow only through 1 mm^2 of the polymer-deposited device region. The measured electrical characteristics indicated high-quality ohmic contact, and the I-V curves were linear. The device was shipped to Prof. Ed Nowak at UD for magnetic and spin-precession measurements. The linear I-V curves were confirmed at RT. As the temperature was lowered, the measured current reduced drastically, possibly because of polymer shrinkage resulting in loss of contact. Further tightening of the screws to obtain good contact increased the measurement current. However, the device current increased as the temperature was further lowered, showing a metallic behavior. If the current flows through the polymer, which is a semiconductor, the current should decrease when T is decreased. This clearly indicates that the tightening process resulted in making direct LSMO-to-LSMO contact on a small area, and neither spin precession nor magnetoresistance measurements can be expected.

In the next iteration to fabricate devices, we addressed the issues related to polymer/LSMO interface, polymer thickness and its dependence of temperature, and clamp design. To solve these issues we conducted a careful and methodical study of polymers, deposition, surface characterization, electrical evaluation, and clamp designs. The study required development of a number of process steps and their integration, as well as a significant amount of characterization to identify the portions of the fabrication process to be corrected in the case of a nonfunctional device. Our study identified the following processes to be addressed:

1. The LSMO needs to be of high quality in structural and electrical properties: flat, high crystal quality, uniform thickness, low and uniform resistivity, and free of defects and particles.
2. The metallization needs to produce an ohmic contact with low contact resistance to the LSMO, remain adhered to the LSMO through further processing and cryogenic testing, and provide a surface suitable for wire bonding so that the electrical signals can reach the outside world. It must be deposited, patterned, and/or etched in such a way as to not destroy or degrade the LSMO and LSMO surface where the P3HT polymer interface will be. That patterning process will likely expose the LSMO to organic solvents and basic photoresists and photoresist developers.
3. The P3HT must also be deposited dissolved in a solution, dried, and patterned on the LSMO without degrading the LSMO. Since the P3HT is the active layer, it must be uniform, flat, and of consistent thickness across the entire device; free from pinholes, particles, and bubbles; and of consistent interfacial electrical properties on the LSMO.
4. The top piece of LSMO must make intimate contact with the now dry P3HT and have the same properties as the other interface. The two LSMO pieces must be parallel so that the thickness of the P3HT is uniform over the entire area of the active device. This sandwich structure must remain intact, with no degradation caused by wire bonding and mounting in the test fixture, shipping and handling at UD, mounting in the test system, or exposure to high magnetic fields and cryogenic temperatures.

To develop an integrated process to fabricate devices to meet all these needs, we adopted the semiconductor industry practice of using “short loops” to proof out portions of the process flow. Essentially the term “short loops” is used to denote a subset of the full fabrication process flow (“steps”) to develop, characterize, test and de-bug segments of the process flow in manageable and deconvoluted pieces.

The high-quality LSMO layers grown at UCR addressed the Process 1 above. The metallization (chromium adhesion layer with a thicker gold top layer) had worked in the past, and Process 2 above is considered a low-risk. Hence, the critical issues are related to Processes 3 and 4. We focused on producing thin, well-controlled layers of P3HT first on Si substrates. Then we reproduced those layers between two layers of cobalt to allow us to make electrical and magnetic

measurements. Once the P3HT process was characterized and understood, we fabricated final LSMO/P3HT/LSMO final devices

Since the deposition and properties of the P3HT polymer are key to the device functionality, the polymer-to-LSMO interface has to be clean and make intimate contact. The polymer thickness must be carefully controlled so that it is between500 nm and 1000 nm. The deposition process involves drop-casting, where a drop of P3HT in a 2% solution in dichlorobenzene, DCB, is placed on the trench and the solvent evaporated. The total device thickness is determined by the trench width and not by the polymer film thickness. The polymer film thickness determines the thickness of the interlayer between the LSMO layers and must be controlled.

We then addressed the issues related to total thickness variation (TTV) across the mm^2 of area. Cleanliness is very important, as dust particles >500 nm in size will change the distance between the two LSMO plates and potentially cause both electrical opens and shorts. Finally, the LSMO interface to the P3HT on the "wet" side may not have the same characteristics of the later LSMO applied to the dry polymer top surface. Therefore, considerable attention must be paid to the deposition method of the P3HT.

We chose to deposit the P3HT film by spin-coating, which is the same process used to coat wafers with thin layers of photoresist for lithography. We carried out a set of experiments to determine the process parameters to attain a polymer film of the appropriate thickness.

One of the parameters is spin speed. Normal processes using spin speeds of 3000 to 5000 rpm are based on the viscosities of commercially available photoresists. In our case, the 2% solution produced films of <20% of the desired final thickness. Reducing spin speeds to 1000 rpm helped, but was not sufficient. Also, we found that filtering syringes are needed to remove particles in the solution. In addition, our chip size of a few millimeters produced defects during spinning due to the interaction with the air and edges. We addressed these issues by designing and machining a recessed holder to use during spinning to minimize these effects as much as possible (Figure 18). Not all edge "beads" need to be eliminated, as they will be etched away during subsequent patterning processes.

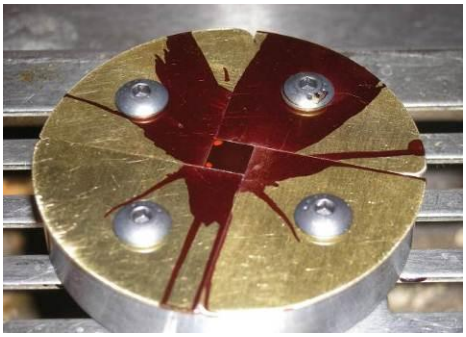

Figure 18: Custom die holder for P3HT spin uniformity improvement. The holder reduces air turbulence and edge scatter of square die at high speeds (>1000 rpm).

We then used the industry standard thickening technique of double-spin coat—spin film, evaporate solvent, reapply solution, spin, and evaporate solvent again. However, the polymer dissolved readily in the solvent of the second spin and the thickness did not increase significantly. Hence we discontinued this approach and undertook the method that employs

higher polymer loading. In this approach, the increased polymer loading in the solution increases the solution viscosity. We increased the polymer loading to 8% from the initial 2% and found that a spin rate of 1500 rpm results in a reasonable quality polymer film.

We then explored the effects of various fabrication and lithographic processes on the LSMO surface. We exposed LSMO to various process steps containing acetone, photoresist, photoresist developer, PECVD oxide deposition, and HF containing wet etchants. Visible inspection of the LSMO indicated that it was mostly unaffected by these processes. Their effects on electrical and magnetic properties need to be evaluated.

Below we summarize all the experimental investigations completed to date and our conclusions.

1. P3HT thickness: The goal is to achieve a > 0.5-μm-thick P3HT device.
   a. Spin conditions (standard 2% P3HT) required sample holder development for edge bead control. Spin speeds greater than 1500 rpm resulted in thicknesses of less than 0.1 μm; spin speeds less than 1000 rpm resulted in nonuniform layers.
   b. P3HT concentrations (custom made by chemist at SRI)
      i. 2% P3HT resulted in thin layers as described above
      ii. 4% P3HT resulted in 0.17 μm at 1500 rpm
      iii. 8% P3HT resulted in 0.33 μm at 1500 rpm
2. Integrated flow development: The goal is to identify P3HT-compatible processes.
   a. We studied the reactivity of P3HT to acetone, developer, BOE (for oxide hard mask patterning), and O_2 plasma and found that P3HT is reactive to acetone, but not to developer or BOE, and that O_2 plasma completely removes P3HT.
   b. We considered development of a compatible pattern mask. The options were to use only photoresist or hard mask. The photoresist option is easier to employ, but the effect of various chemicals on the polymer needs careful and detailed evaluation. We chose the hard mask option, which involves evaporation of oxide, deposition of resist for patterning, HF etch of oxide and then O_2 plasma to etch P3HT to obtain a patterned polymer on LSMO (Figure 19).

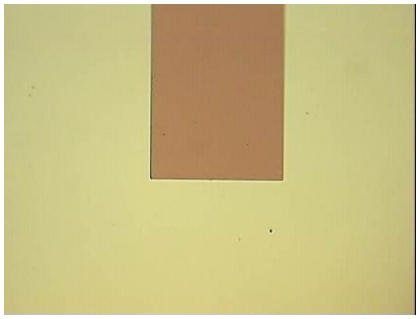

Figure 19: P3HT rectangle in a field of Au in the background post patterning with integrated O2 plasma process.

   c. Development of a well-studied test structure using cobalt required custom Co crucibles with several thickness and rates to achieve 30-nm-thick Co layers. We have fabricated one Co/P3HT/Co device (Figure 20). The measured current-voltage (I-V) curve (Figure 21) is clearly linear and indicates good ohmic contact between the polymer and Co. Its magnetic and spin properties at very low temperature are currently being evaluated at UD. We will compare our results with the published results to validate our fabrication and measurements.

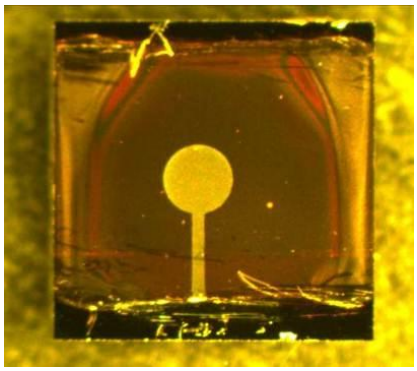

Figure 20: Co/P3HT/Co device. Focal plane is top Co deposition. Black edges are Au pads for probing and bonding the device to UD carrier chip. Scratches were from manual short tests. Blanket P3HT manually removed from edge Au bond regions, no lithography.

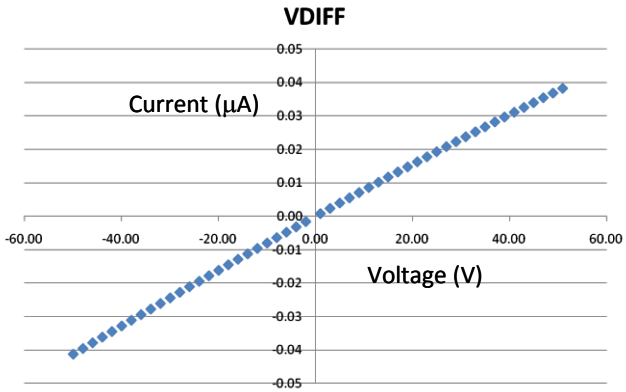

Figure 21: Measured current-voltage characteristics of Co/P3HT/Co device.

The detailed process studies and Co device fabrication studies enabled us to arrive at a process flow for the fabrication of the LSMO/polymer/LSMO magnetic sensor device. Figure 22 shows a typical device. The crossbar holds the top and bottom LSMO pieces together. The electrical contacts are connected to a chip carrier for convenience of testing and transportation. For comparison, we had also fabricated a monolithic device consisting of Co/P3HT/Co, where the top FM layer of Co is evaporated on the polymer. This device is expected to have a near-perfect interface between the polymer and the FM layers. The measured I-V curves shown in Figure 21 for the Co device indicate that the I-V is nearly linear in the monolithic device in which the top Co is evaporated on the polymer.

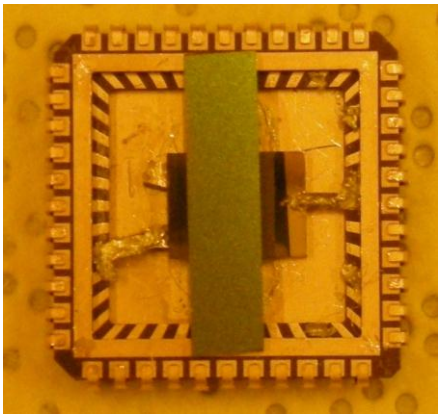

Figure 22: Typical vertical device.

In the I-V curves for the LSMO device shown in Figure 23, the I-V response was measured first at RT before and after pressing the top and bottom LSMO plates together; then at liquid nitrogen temperature (LN) of 77 K; and finally again at RT. As seen from Figure 23, the I-V curve changes with time when measured at 77 K, but is nearly unchanged after a thermal cycle to yield similar I-V at RT. However, all curves are nonlinear (i.e., resistance change with the applied bias), indicating poorer polymer/LSMO interface. When the contact is non-ohmic, the charge injection is through tunneling, and the I-V curve will be nonlinear.

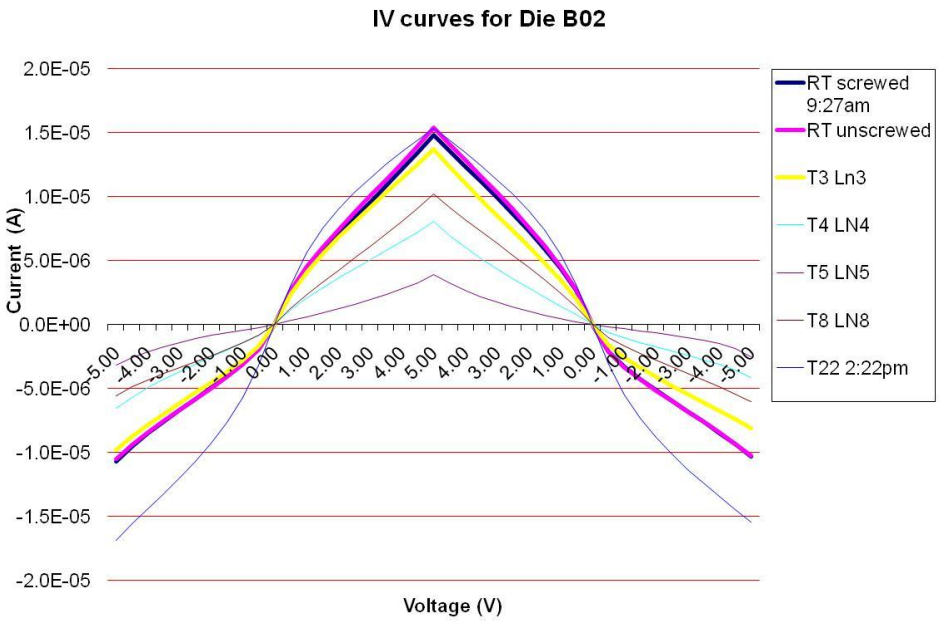

Figure 23: Measured I-V curves from LSMO/P3HT/LSMO device.

We next shipped the device to UD for electrical and magnetic measurements. The measured resistance (R) at 1 V of bias is plotted in Figure 24 as a function of time. The value measured at SRI is shown by a red dot. The same device yielded a higher resistance at UD (denoted "As made-UD") and decreased as a function of time. When that device is annealed for curing the polymer, the resistance dropped, but continued to decrease (denoted "Cured-UD") with time. The same device measured again at SRI after a few days showed higher resistance initially and a steady-state lower resistance with time. These variations clearly indicate that the polymer is being doped from the environment. Therefore, encapsulation will be needed for reliable device performance, which could be accomplished in future versions.

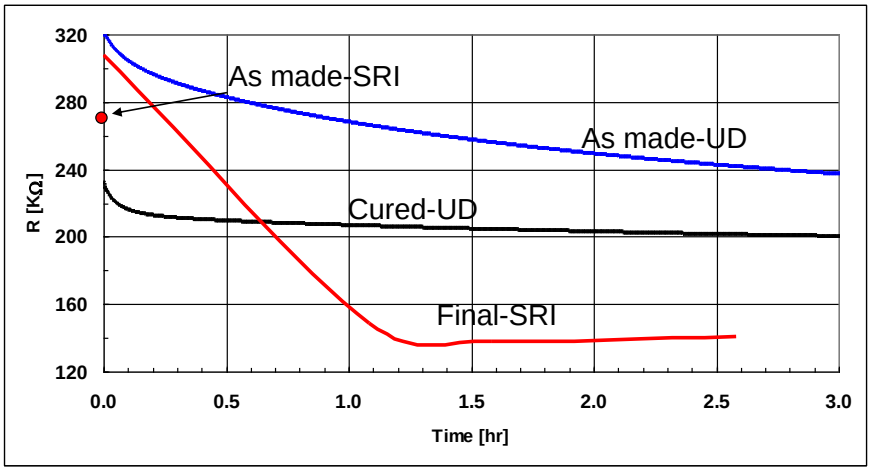

Figure 24: Measured change in electrical resistance with time.

Finally, we measured the LSMO device's magnetic response and the measured change in MRI and plotted them as a function of magnetic field sweep (Figure 25). Since the measurements are carried out over a period of ~3 h, the base resistance changes with time (as described above). More important, the periodic oscillation in MR associated with spin precession with a period of about 10 mG (0.001 mT) is not observed. If the RT magnetization and spin polarization of the LSMO contact is high, then the change in MR will be much higher than the noise inherent in polymer devices. Currently the signal, if any, is overwhelmed by noise, as seen in Figure 25. The magnetization at RT is very small, owing to low T_c, and, consequently, smaller spin polarization. Further, the sandwiched devices appear to have a poorer interface, resulting in diode-like, rather than ohmic, behavior. The lack of high spin injection at RT along with the effect of poorer interface on local measurements makes the vertical LSMO devices not useful for RT magnetic sensing devices.

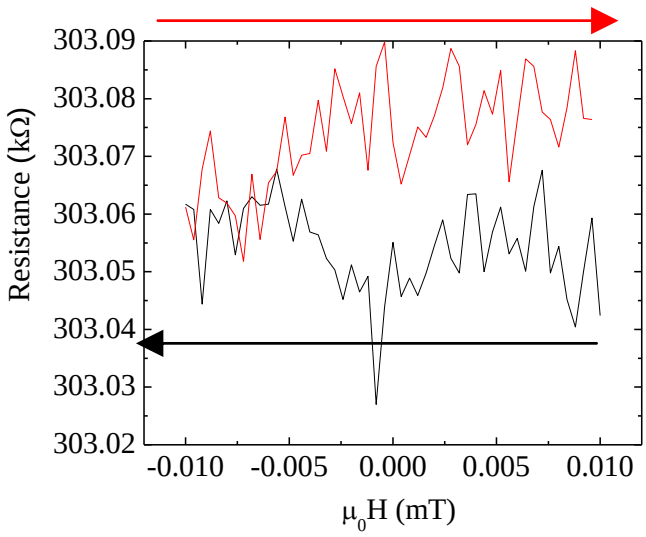

Figure 25: Measured magnetoresistance at room temperature.

6. CFAS Device Results

We fabricated lateral devices with CFAS so that we could study sequentially both local and nonlocal configurations. The fabrication process and schematic designs are described above. The devices were subjected to an external H field and the resistance measured from the I-V curves. The measured I-V characteristics were found to change with time, even in the absence of applied magnetic field, and the change was often larger than the expected signal. We improved the SNR by AC-lock in measurements, as shown in Figure 26, in which an AC signal of known frequency (often at 10 Hz) is superimposed on input DC voltage and the change in the output is measured only with reference to AC input for local (left) and non-local (right) configurations. The output voltage is measured between terminals 3 and 4 in the nonlocal configuration, and between terminals 1 and 2 in the local configuration.

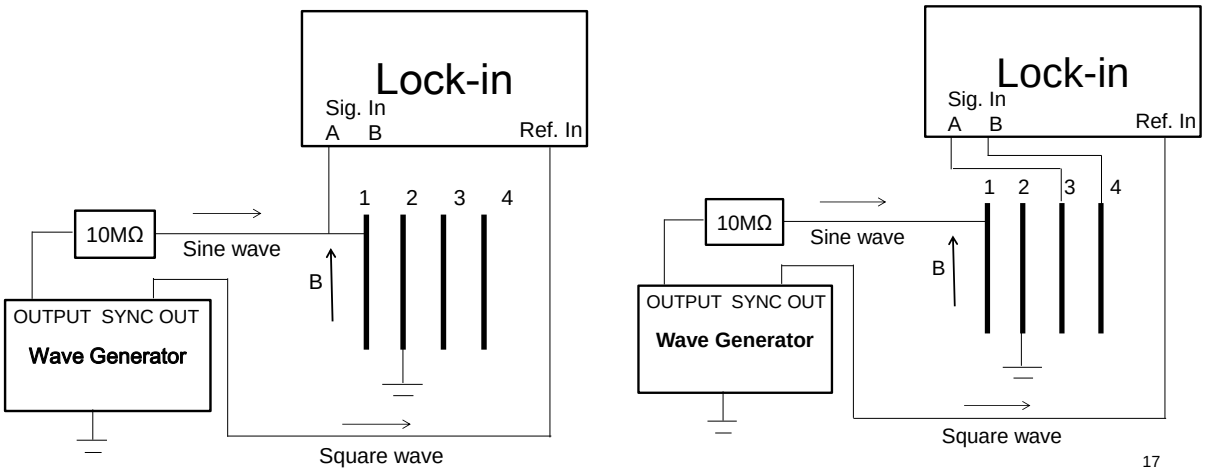

Figure 26: AC lock-in for improved SNR in local (left) and nonlocal (right) devices.

We carried out both local and nonlocal magneto resistance measurements on all the devices. The measured resistance at RT either did not change or changed repeatably with applied magnetic field. Ideally, the response should be similar to the spin-valve measurements—the resistance changes as the magnetization of each of the contacts flips as we sweep the H field. However, a typically observed variation of measured voltage as a function of applied H field is shown in Figure 27 for local (left) and nonlocal (right) device. The field is varied from 0 G to 500 G (step 1, blue), 500 G to 0 G (step 2, red), 0 G to -500 G (step 3, green), -500 G to 0 G (step 4, violet) and again 0 G to 500 G (step 5, cyan). In the local configuration (left), very little change is seen in all sections of variation. Our AC lock-in design is better able to suppress the noise in local than in nonlocal configuration.

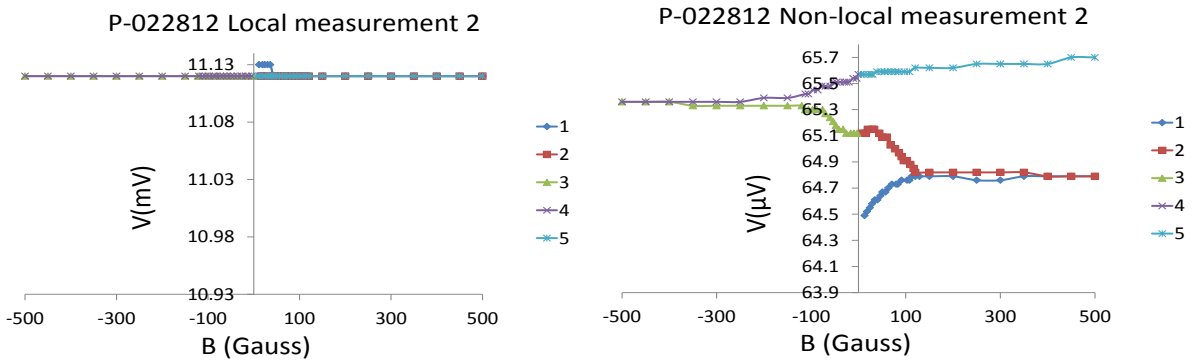

Figure 27: Measured electrical response to applied magnetic field in local (left) and nonlocal (right) configurations.

Assuming the lack of spin injection could be because of lower spin polarization at 300 K, we measured magnetoresistance at 120 K, 77 K, 35 K, and 4.2 K. None of the devices exhibited reliable and repeatable magnetoresistance. Since the source is well spin-polarized at low temperature, we conclude that spin injection has not been achieved in these devices.

7. Conclusions and Recommendations

Since the LSMO deposition temperature is much higher than the polymer melt temperature, we tried a two-piece device approach for vertical LSMO devices. The sandwich structure devices have a poorer interface between the top LSMO plate and the polymer. The charge injection was dominated and limited by uncontrollable interface quality, and both electrical and magnetic measurements were nonlinear and noisy.

One of the LSMO devices studied in the lateral architecture and in local configuration showed evidence of spin injection and precession, but only at the low temperature of 25 K. The measurements were repeated over long periods of time and responses were nearly identical. However, at high temperatures, the responses were noisy because of (a) low RT spin polarization at the surface, (b) polymer being auto-doped from the environment, (c) low signal owing to small device area.

Since the Curie temperature of LSMO is around 360 K, the spin-polarization at RT is not high enough for efficient spin injection. CFAS has been predicted to have high Curie temperature (~1000 K) and high spin polarization (~0.9) at RT. Our PLD-grown and sputtered CFAS films do confirm very large Curie temperature, high and temperature-independent coercive field and magnetization. However, careful, systematic, and direct measurements of surface spin polarization indicate that the polarization factor is ~0.73. While this is the highest ever directly measured value for any FM material, it is not high enough to overcome the resistance mismatch without an oxide tunnel barrier. Consequently, sufficient spin injection has not been achieved to observe magnetoresistance in either local or nonlocal configurations at any temperature. We tried a few samples with controlled Al_2O_3 thickness and a few with natural oxide. The samples with Al_2O_3 showed very little tunneling because the thickness has not yet been optimized. The samples with thick native oxide showed sufficient tunneling, but the carriers were interacting with the barrier and lost spin coherence.

SRI recommends that further studies to improve spin injection efficiency include the following steps:

(a) *Optimize the Al_2O_3 barrier layer to achieve resistance match.* The controlled growth of the oxide layer on CFAS is straightforward. We will then measure the I-V curve as a function of barrier layer thickness, and the effective contact resistance can be calculated. For the known polymer layer thickness and mobility, the doping can be varied to obtain a resistance match to the contacts.

(b) *Control the choice of oxide for the barrier.* The impurities in the oxide layer can depolarize the spins while tunneling. The variation of measured tunneling conductance with bias offers evidence to support this possibility. Since native oxide is present in all our

devices, spin injection is destroyed. This can be corrected by performing Ar^+ sputter-etching for 5 min on the CFAS surface before depositing a well-controlled Al_2O_3 layer.

(c) *Verify size-dependence of coercive field of CFAS lines.* The size-dependent coercive field is normally exploited to independently orient the magnetization of the contact strips. Typical spin-valve measurements employ strip widths of ~10-20 nm. However, the smallest width achievable in our FIB process is 500 nm, and the coercive field of this thin strip is not independently measured to be different from its bulk value. Future fabrication should explore depositing thin lines of CFAS. While size-dependence is not needed for the operation of spin precession magnetic sensor operation, it will allow the device to operate in an anti-parallel configuration. In this configuration, the dark current will be nearly zero, leading to extremely small power consumption and magnetic field sensitivity very high.